

Bridging the View Disparity of Radar and Camera Features for Multi-modal Fusion 3D Object Detection

Taohua Zhou, Yining Shi, Junjie Chen *Member, IEEE*, Kun Jiang, Mengmeng Yang, and Diange Yang

Abstract—Environmental perception with multi-modal fusion of radar and camera is crucial in autonomous driving to increase the accuracy, completeness, and robustness. This paper focuses on how to utilize millimeter-wave (MMW) radar and camera sensor fusion for 3D object detection. A novel method which realizes the feature-level fusion under bird-eye view (BEV) for a better feature representation is proposed. Firstly, radar features are augmented with temporal accumulation and sent to a temporal-spatial encoder for radar feature extraction. Meanwhile, multi-scale image 2D features which adapt to various spatial scales are obtained by image backbone and neck model. Then, image features are transformed to BEV with the designed view transformer. In addition, this work fuses the multi-modal features with a two-stage fusion model called point fusion and ROI fusion, respectively. Finally, a detection head regresses objects category and 3D locations. Experimental results demonstrate that the proposed method realizes the state-of-the-art (SOTA) performance under the most important detection metrics—mean average precision (mAP) and nuScenes detection score (NDS) on the challenging nuScenes dataset.

Index Terms—Multi-modal fusion, Object detection, Intelligent driving, Automotive radar, Camera.

I. INTRODUCTION

INTELLIGENT vehicles are usually equipped with multiple sensors to enhance the environment perception ability for safety. While LiDAR perception methods have obtained wonderful performance with precise 3D measurement, the expensive cost of LiDAR makes it hard to be applied for large-scale deployment on intelligent vehicles. Compared with LiDAR, camera and radar units are easier to be accepted and radar-camera fusion has been widely applied in the Advanced Driving Assistance System (ADAS) for intelligent vehicles. MMW radar can provide direct object measurement of relevant object position and velocity, robust to adverse weather conditions, and in low cost [1]. However, radar point clouds lack semantic information and can not avoid clutter from the environment. Camera images own abundant semantic information about the environment but are quite sensitive to light and occlusions. Therefore these two sensors can complement each other and exploit the advantages of both sensors. However, as multi-modal measurements are represented in heterogeneous space, multi-modal fusion detection is more complex than single-

sensor perception. And there still exist some problems to be explored.

In general, there are three kinds of radar-camera fusion schemes to solve fusion-based object detection. The first fusion scheme is output fusion which fuses the single-sensor detection output for a higher-confidence result with the D-S evidence theory [2] or fusion filter algorithm [3]. This kind of method can not exploit raw sensor data adequately and is quite dependent on the probability modeling of single sensor result. The second fusion framework is raw data fusion which usually projects radar points to the image plane. Then projected radar data provide hints of the region of interests (ROIs) for further feature extraction to get higher precision and recall [4] [5]. This kind of fusion algorithm is more suitable to boost 2D image object detection rather than describe 3D environment information. Besides, the giant difference between radar and camera data structure makes fusion at low dimensions quite tough. The third one, which is called feature fusion, exploits Deep Neural Networks (DNN) to fuse high-dimensional features generated from radar data and images. This kind of framework can fully exploit the intermediate features from raw sensor data and the fusion model can be designed to solve various regression problems, including 2D image bounding box estimation, 2.5D (2D image bounding box and depth estimation), and 3D object detection [6] [7] [8].

Feature fusion methods based on radar-camera data are mainly implemented in the following paradigm [8] [9]. Firstly, image features are extracted by Convolutional Neural Networks (CNN) of the image branch and radar points are explored to generate radar feature maps under the image view according to the designed rule. Next, a fusion network is explored to fuse the two-branch multi-modal features in the same spatial-temporal reference system. Then locations and categories of objects are regressed through an anchor-based or anchor-free detection head. However, as the camera captures semantic information in the front view and radar obtains spatial information in the 3D space, directly projecting radar points to the image plane through a calibration matrix which ignores the distinction of information presentation, especially the view discrepancy of different sensors. This kind of fusion method causes the loss of high-dimension information from different sensors for 3D perception task, which impacts the fusion effect consequently. Lim et.al. were also aware of this problem and devised an Inverse Projection Mapping (IPM) method to realize image information presentation under the same space with radar [10]. Then their fusion network extracts

T. Zhou, Y. Shi, J. Chen, K. Jiang, M. Yang, and D. Yang are with State Key Laboratory of Automotive Safety and Energy, School of Vehicle and Mobility, Tsinghua University, Beijing, China (e-mail: ydg@mail.tsinghua.edu.cn; jiangkun@tsinghua.edu.cn; junjie@tsinghua.edu.cn).

Manuscript submitted August 22, 2022

and fuses camera and radar features for better detection performance. However since direct IPM will cause distortion and loss of image features, realizing spatial-temporal synchronization at the raw data stage may not be the most suitable approach for feature-fusion detection.

According to the discussion above, to avoid information loss, it is necessary to consider the representation of fusion features suitable to combine the characteristic of 3D radar points and image information respectively. The success of visual perception work under BEV, also called the top-down view, such as lift-splat-shoot [11] and BEVDet [12], gives us some heuristic information. We consider representing the cross-view features to realize spatial-temporal synchronization rather than using raw data. Besides, When we visualize radar point clouds and object 3D bounding box under bird-eye view, we find that radar point clouds are distributed among the object edge. We intend to use this geometry constraint to enhance the fusion performance. Therefore we design a two-stage fusion method called point-fusion and ROI-fusion to fully exploit the multi-modal information. What's more, considering the sparse and clutter of radar points, a temporal-spatial feature extractor is introduced to process radar data.

This paper will introduce a cross-view feature-level fusion framework which is called RCBEV utilizing radar and camera data to realize 3D object detection. With the proposed radar temporal-spatial encoder, efficient features are extracted by overcoming the sparsity and clutter of radar points. Through a designed multi-scale view transformer, cross-view fusion feature representation is obtained. Then a two-stage fusion scheme is realized. Point-fusion at the intermediate feature stage and ROI-fusion at the high-dimensional feature stage are proposed. Finally, 3D detection results are acquired with an anchor-free regression head. The main contributions of our work lie in three parts:

- 1) A novel 3D object detection network for feature-level radar-camera fusion is proposed. To the best of our knowledge, we are the first to bridge the view disparity of multi-modal features for radar-camera fusion detection. Cross-view fusion features are exploited to avoid information loss and two-stage fusion modules are designed to exploit multi-modal features adequately.

- 2) A temporal-spatial encoder is designed to process radar data and deal with the sparsity and clutter of radar point clouds. Besides, considering the geometry constraints provided by radar, high-dimensional heatmaps are generated to enhance the spatial information regression compared with vision-only networks.

- 3) The effectiveness of our proposed framework is verified on the nuScenes dataset. Extensive experiments are carried out to prove the overall effectiveness of RCBEV and its robustness under the special situations. We realize the SOTA under camera-radar modality under the nuScenes leaderboard.

The rest of this paper is organized as follows. Section II presents an overview of key previous studies. Section III introduces the overall architecture of RCBEV. Then Section IV explains the detailed algorithm design. Experiments are conducted and analyzed by using the public autonomous driving dataset nuScenes in Section V. Finally, conclusion of this

proposed work is summarized in Section VI.

II. RELATED WORK

A. 3D Object Detection

With the precise 3D spacial information measured by LiDAR sensors, related 3D object detection methods greatly developed at first. Two-stage detectors such as PointRCNN [13], and PV-RCNN [14], single-stage LiDAR 3D detectors such as Voxelnet [15], and PointPillars [16], and anchor-free detectors such as CenterPoint [17], and Object DGCNN [18] have achieved brilliant performance.

Due to the high cost of LiDAR, camera-only 3D perception also followed close on another. Unlike LiDAR sensors, lack of depth cause difficulty to image 3D detection. The solutions are mainly divided into the following types. The earliest works tried to import geometry prior information and camera model to get 3D information [19]. However, these proposals are quite easily impacted by occlusion, truncation, and height estimation errors. The second attempt is to utilize image features with additional depth information to produce pseudo LiDAR point clouds and get the final detections using network models to process the point clouds [20]. The third type extends the 2D image detector with additional 3D regression branches such as FCOS3D [21], and CenterNet [22]. The fourth design is the deformable-transformer-based detection method with learnable object queries to get 3D object information such as DETR3D [23] and PETR [24]. The last and the most concerned ones present a view transformer and project image-view features to BEV, such as Imvoxelnet [25], BEVDet [12], and M²BEV [26]. Up to now, multi-images 3D detection is the most concerned in this research field.

B. Radar-Camera fusion Object Detection

With the development of image 2D detection paradigm, such as Faster RCNN [27] and YOLO [28], researchers explore to utilize more data augmentation to improve the detection performance when there exists occlusion or when in raining environment or dark night. SAF-FCOS [7], CRF-Net [29], RVNet [30] and other studies have acquired convincing evidence to prove that radar data can help to further promote the detection performance of camera image under these special scenarios.

Moreover, with the development of 3D image object detection, CenterFusion [8] realized 3D object detection based on radar-camera feature fusion and proved that the result surpass the result of baseline image detection model CenterNet [22]. However, how to deal with the sparsity of radar data and reduce the noise or clutter in radar data when processing radar data [31] [32], and how to utilize the different-modal data to realize efficient feature representation when implementing fusion-based perception task are the two key issues all the time.

III. SYSTEM ARCHITECTURE

This work aims to build an efficient approach by bridging the view disparity between radars and image features and

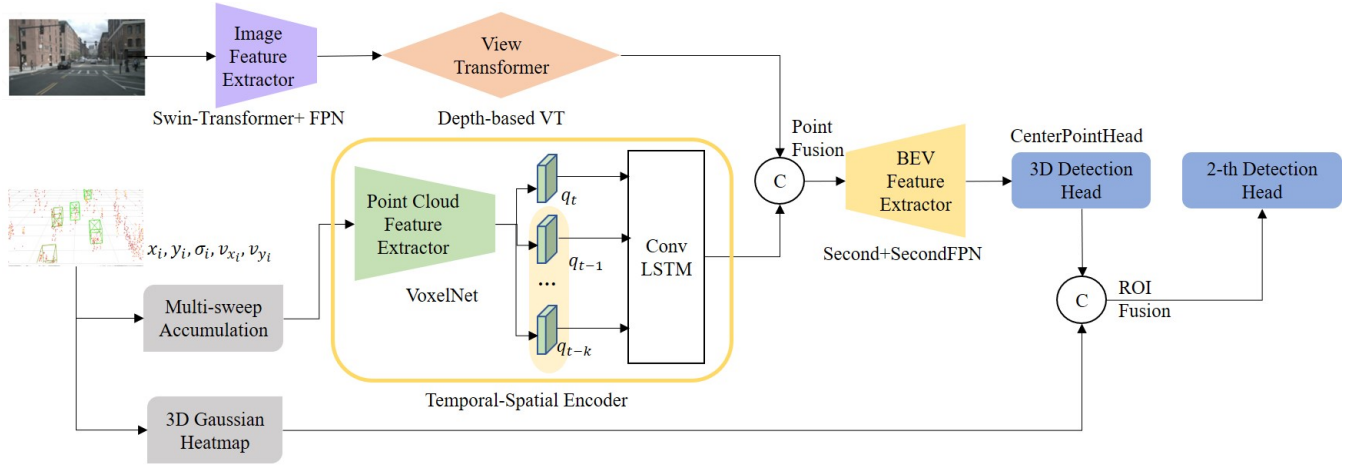


Fig. 1. Overview of the proposed RCBEVDet for 3D Object Detection

designing a multi-modal feature fusion method to enhance the 3D object detection performance compared with single sensor results for autonomous driving vehicles. The overview of the proposed end-to-end system architecture is illustrated in Fig 1.

At first, multi-scale features under image view are extracted through a well-performed backbone network such as Swin-Transformer [33] and a neck model such as Feature Pyramid Network (FPN) [34]. Then image-view features are then transformed to BEV space at pixel level with a designed view transformer.

Meanwhile, this paper proposed a specific scheme to deal with the sparsity and clutter of radar points. Firstly, single-frame raw data from radar needs some preprocessing. Multi sweeps of radar points are accumulated with vehicle localization information to overcome data sparsity. A confidence filter is designed to cover clutter and false alarms. Secondly, a temporal-spatial encoder is proposed. Unlike 3D outdoor measurements, radar points only provide 2D location information x_r and y_r with no height information. To enrich radar features, ego-motion compensated Doppler velocity v_r and the radar cross section (RCS) σ which reflected signal intensity are also utilized. Then the 4-dimensional data are sent to the spatial processing module, similar to the one-stage LiDAR point cloud detection backbone model. And a ConvLSTM model is used to extract temporal information [35].

As for the fusion module, we design a two-stage fusion strategy for a sufficient multi-modal feature interaction. Image features from bird-eye view and radar features under the same space are fused with convolution layers at the point-fusion stage. Then we realize ROI-fusion which means region-of-interest-fusion to further refine the 3d location and dimensions of objects. We use radar object list to generate heatmaps which obeys Gaussian distribution under 3D space to reflect the geometry constraints of objects under BEV. The augmented high-dimensional heatmaps are then used to regress categories and 3D bounding boxes with a 3D detection head.

IV. METHODS

In this section, the end-to-end cross-view 3D detection model fusing radar and camera data at the feature level will

be introduced. Our RCBEV model mainly consists of 4 parts: Radar branch, image branch, fusion branch, and detection head. We emphasize on the structure design of each part in the following content.

A. Radar processing

To fully exploit radar features for 3D object detection and handle the sparsity and clutter, temporal information is imported to enlarge the useful radar information. Besides, as two-stage fusion algorithm is competent for a more effective result, we try to express low-dimension and high-dimension radar features for two fusion tasks, respectively. Consequently, three modules are specially designed: 1) data preprocessing module 2) radar feature spatial-temporal encoder 3) object heatmap generator.

In the data preprocessing module, we realize a multi-sweep integrator and clutter filter to ensure the quality of training data. Based on sensor calibration parameters, global localization information, and timestamp of sensor data recording time, multi-sweep radar points can be unified at current frame under the reference coordinate system. The mathematical formulation of the above course is listed as

$$\mathbf{Z}_r^{ref}(t) = \mathbf{T}_{ego}^{ref}(t) \mathbf{T}_{global}^{ego(t)} \mathbf{T}_{ego(t-k)}^{global} \mathbf{T}_{radar}^{ego(t-k)} \mathbf{Z}_r^{radar}(t-k) \quad (1)$$

In (1), $\mathbf{Z}_r^X(t)$ denotes radar measurements at timestamp t under X coordinate system, while \mathbf{T}_Y^X denotes the transformation matrix from Y coordinate system to X coordinate system. It is made up of rotation matrix \mathbf{R}_Y^X and translation vector \mathbf{t}_Y^X as is shown in (2).

$$\mathbf{T}_Y^X = [\mathbf{R}_Y^X | \mathbf{t}_Y^X] = \begin{bmatrix} \mathbf{R}_Y^X & \mathbf{t}_Y^X \\ \mathbf{0} & 1 \end{bmatrix} \quad (2)$$

The clutter filter is designed to evaluate the confidence of radar points according to their dynamic properties, intensities, and probabilities of being objects. The points which are not satisfied with the conditions are filtered out.

Our radar feature spatial-temporal encoder is constructed to extract radar features at a higher dimension. As is shown

in Fig IV-A, four-dimensional information from radar point clouds, including radial distance x_r , lateral distance y_r , ego-motion compensated Doppler velocity v_r and the RCS value δ are input data. We import existing 3D encoder detection backbones including VoxelNet [15] and PointPillars [16] to extract radar point features. Then the features are sent to ConvLSTM, a kind of Long Short-Term Memory network which uses convolution operations to extract 2D sequential features.

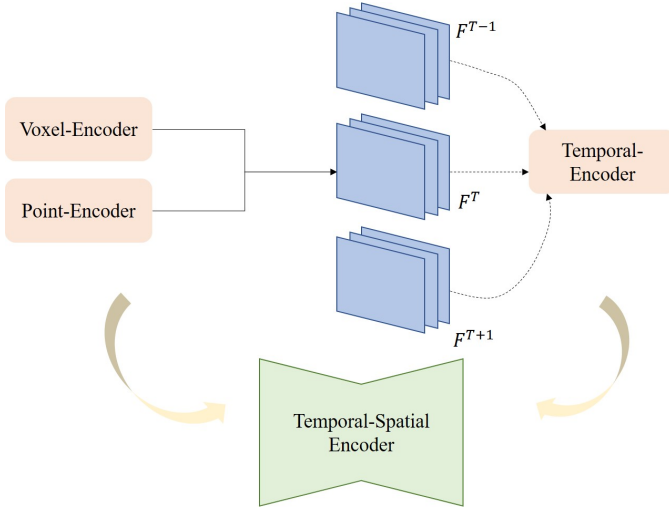


Fig. 2. Illustration of radar data processing

Finally, radar heatmaps expression $\mathbf{H}_i(x, y)$ which will be introduced in Sec IV-C are generated. To construct the heatmaps with Gaussian distribution, the mean value is denoted by radar position measurement p_x and p_y , the standard deviation is a function of width w and length l measured by radar: $\sigma = \max\{f(wl), \tau\}$. When generating the multi-channel heatmaps, raw data such as position, intensity, velocity, and false alarm probability of cluster are considered to determine M_i , the amplitude-related parameter. Therefore we set $i = 6$.

$$\mathbf{H}_i(x, y) = 1/M_i \begin{cases} e^{-\frac{(x-p_x)^2+(y-p_y)^2}{2\sigma_i^2}} & |x-p_x| \in 3\sigma, \\ & |y-p_y| \in 3\sigma \\ 0 & \text{otherwise} \end{cases} \quad (3)$$

B. Image processing

The image branch provides important semantic information in RCBEV and is divided into three parts: 1) image-view feature extractor 2) cross view feature transformer 3) BEV feature extractor.

The image-view feature extractor is designed to extract multi-scale image features which are suitable for detection. A good backbone network with a suitable neck model is important to the performance of image-related perception tasks. Here we select some excellent backbones such as ResNet [36] and Swin-Transformer, etc.

The cross View transformer is the crucial part for bird-eye-view image-related tasks. It is constructed to project image features from a front-view perspective to a bird-eye-view

perspective. Considering that directly IPM method, which projects image features to BEV with a homography matrix, is based on an assumption of flat ground, it often causes distortion of dynamic objects in the real environment. What's more, it is easily impacted by the turbulence of vehicles or roads. Therefore we adopt another scheme which is similar to lift-splat-shoot. We use image-view features to conduct vision frustum which reflects semantic features with depth estimation. Then with extrinsics and intrinsics of camera, features expressed in vision frustum are splatted to the reference space under BEV where radar and image features will be synchronized.

The BEV feature extractor is arranged to further extract features to fit the information representation under the top-down view. We use the basic layers of Resnet and FPN to operate this module.

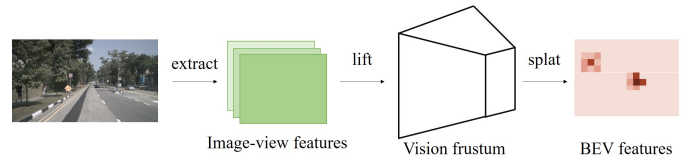


Fig. 3. Illustration of image data processing

C. Fusion module

To realize a sufficient feature interaction during the fusion process, a two-stage R-C fusion method is put forward. Based on the operation order in forward propagation, the two fusion mode is called point-fusion and ROI-fusion, respectively.

This paper fused the different sensor-branch features at the point-fusion stage under the same bird-eye-view space shared by radar and camera features. As the two-branch features have been presented as the form of pseudo-LiDAR point clouds, the fusion stage is called point-fusion. This paper used the downsampling and upsampling operation to unify the resolution of different feature maps. Then a classical convolution layer with Batch Normalization (BN) and activation layer with ReLU function is applied to fuse the image features which are processed after the BEV feature extractor and radar features which are processed after the radar temporal-spatial encoder.

Then a shared convolution layer is used to obtain the prediction heatmaps of different categories. Radar feature heatmaps, which are mentioned in Sec IV-A, are fused with this detection heatmap to realize the second-stage fusion. As both the high-dimensional features have implied the region of interesting objects in 3D space, this stage is named as ROI-fusion.

D. Detection head design

Our detection head is designed to process the fusion features and get the prediction results of the whole model. As we realize an anchor-free detection model, we use a share convolution layer to calculate the heatmap of objects and regression losses. Then jointly optimize them under BEV.

As for the loss design of our fusion model, there are two branches consisting of object classification and location regression. The loss of them is termed as L_{cls} and L_{reg} respectively. The total training loss for the whole task is constructed as

$$L_{total} = \alpha L_{reg} + L_{cls} \quad (4)$$

Under BEV, features of foreground objects is quite sparse compared with background information, therefore we utilize focal loss form L_{cls} to deal with the unbalanced sample classification. After the former process, all the features are splatted as feature heatmaps \hat{H} of classes c under BEV. We splat ground truth onto heatmaps $\bar{H} \in [0, 1]^{\frac{W}{R} \times \frac{H}{R} \times C}$ as a similar way using a Gaussian kernel $\bar{H} = \exp\left(\frac{((x - \bar{p}_x)^2 + (y - \bar{p}_y)^2)}{2\sigma_p^2}\right)$. And in order to do continuous calculations instead of discrete ones, we use another Gaussian function $\mathcal{G}(\bar{H})$ to present the probability of objects. Then the category loss is calculated as

$$L_{cls} = -\frac{1}{N} \sum_{xyz} \log(\hat{H}) (1 - \hat{H})^\alpha \mathcal{G}(\bar{H}) + \log(1 - \hat{H}) \hat{H}^\alpha (1 - \mathcal{G}(\bar{H}))^\gamma \quad (5)$$

where α and γ are the constants in focal loss design. Here we set $\alpha = 2$ and $\gamma = 4$. C is the number of categories.

As for the loss L_{reg} of 3D information such as location including p_x, p_y, p_z position in 3D space, dimensions including width w , length l and height h of object bounding boxes, velocity including including v_x, v_y , and orientation θ of objects, we follow the L1 loss to regress position offset \hat{O}_p , dimensions, heading angle as L_{off}, L_{dim} , and L_{vel} . We use softmax function to calculate orientation loss L_{rot} which is encoded with two bins b and 8 scalars. Then the Binary Cross

Entropy (BCE) loss is used to calculate attribute loss L_{att} of attributes a .

$$\begin{aligned} L_{reg} &= \lambda_{off} L_{off} + \lambda_{dim} L_{dim} + \lambda_{vel} L_{vel} + \lambda_{rot} L_{rot} + \lambda_{att} L_{att} \\ L_{off} &= \frac{1}{N} \sum_p \left| \hat{O}_p - \left(\frac{p}{R} - \tilde{p} \right) \right|, p = p_x, p_y, p_z \\ L_{dim} &= \frac{1}{N} \sum_{k=1}^N |s_k - \hat{s}_k|, s = w, l, h \\ L_{vel} &= \frac{1}{N} \sum_{k=1}^N |v_k - \hat{v}_k|, v = v_x, v_y \\ L_{rot} &= \frac{1}{N} \sum_{k=1}^N \text{softmax}(\hat{b}_k) + \frac{-1}{n_\theta} \sum_{i=1}^{n_\theta} \cos(\theta - b_i - \Delta\theta_i) \\ L_{att} &= \frac{1}{N} \sum_{k=1}^N \frac{1}{A} \sum_{i=1}^A -w_i |a_k^i \log \hat{a}_k^i + (1 - a_k^i) \log(1 - \hat{a}_k^i)| \end{aligned} \quad (6)$$

where N is the number of training samples, n_θ is the number of bins that cover the heading angle θ , b_i is the angle of the center of bin i and $\Delta\theta$ is the change that needs to be applied to the center of bin i . A is the number of attributes in driving scenes.

V. EXPERIMENT

A. Dataset and Evaluation metrics

Experiments are implemented on the large-scale public dataset nuScenes [37] for research of autonomous driving. Data of 1000 driving scenes were collected in Boston and Singapore in nuScenes. Approximately 1.4M camera images, 390k LIDAR sweeps, 1.4M RADAR sweeps and 1.4M object bounding boxes in 40k keyframes are recorded. Except the common scenes, special scenarios such as rainy day and night are also included in this dataset.

We use the metrics which are designed for the nuScenes detection tasks. There are three kinds of official metrics to evaluate detection performance. First, Average Precision metric is represented by mean Average Precision (mAP) which is calculated for measuring the precision and recall of detection methods. However in nuScenes metrics, it is not defined based on the Intersection over Union (IOU), but the match by 2D center distance on the ground plane. Second, True Positive (TP) metrics is used to evaluate the multi-aspect precision, including Average Translation Error (ATE), Average Scale Error (ASE), Average Orientation Error (AOE), Average Velocity Error (AVE), and Average Attribute Error (AAE) of detection results. Third, nuScenes detection score (NDS) is designed to indicate the all-sided detection performance which consider mAP, and the quality of regression in terms of box location, size, orientation, attributes, and velocity. As in (7), the above metrics are calculated over distance matching threshold of $\mathbb{D} = \{0.5, 1, 2, 4\}$ and the set of ten classes \mathbb{C} .

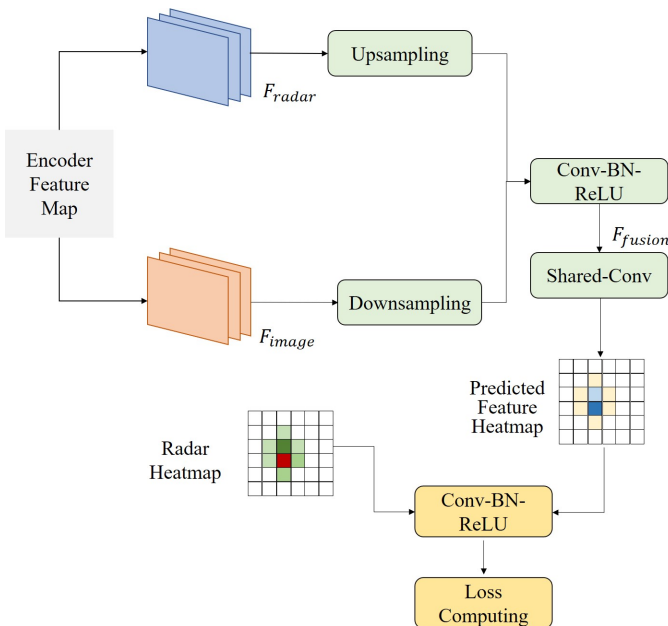


Fig. 4. The structure of fusion network

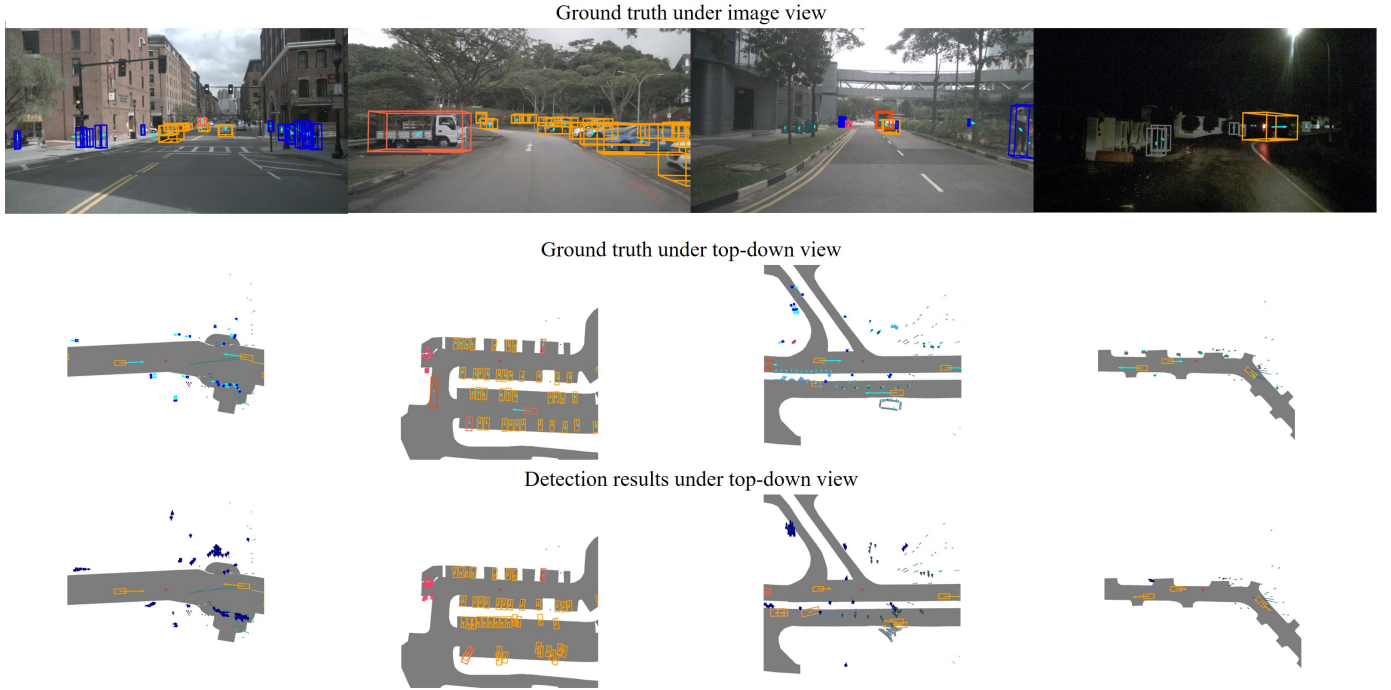


Fig. 5. 3D Detection results on nuScenes dataset of RCBEV with R-C fusion. The pictures from the top to the bottom are labels under image view, labels under BEV, and detection results under BEV. The scenes are in city roads, parking lot, rainy day, and night.

TABLE I
PERFORMANCE COMPARISONS FOR 3D OBJECT DETECTION ON NUSCENES DATASET.

Method	Modality	data	Metric						
			NDS \uparrow	mAP \uparrow	mATE(m) \downarrow	mASE(1-IoU) \downarrow	mAOE(rad) \downarrow	mAVE(m/s) \downarrow	mAAE(1-acc) \downarrow
BEVDet	Camera	val	0.403	0.308	0.665	0.273	0.533	0.829	0.205
BEVDet4d	Camera	val	0.476	0.338	0.671	0.274	0.469	0.337	0.185
RCBEV(Ours)	Camera+Radar	val	0.482	0.377	0.534	0.271	0.558	0.493	0.209
RCBEV4d(Ours)	Camera+Radar	val	0.497	0.381	0.526	0.272	0.445	0.465	0.185
mm-fusion	Camera+Radar	test	0.483	0.371	0.628	0.250	0.513	0.536	0.095
CenterFusion	Camera+Radar	test	0.449	0.326	0.631	0.261	0.516	0.614	0.115
RCBEV(Ours)	Camera+Radar	test	0.486	0.406	0.484	0.257	0.587	0.702	0.140

\uparrow denotes the higher the value is, the better the performance is. \downarrow denotes the lower the value is, the better the performance is. Numbers in bold represent the best performance under this criteria.

Though the mAAE value of BEVDet4d and RCBEV4d remain the same after keeping three decimal places, the raw number of RCBEV4d is smaller than BEVDet4d.

$$mAP = \frac{1}{|C| |D|} \sum_{c \in C} \sum_{d \in D} AP_{c,d}$$

$$mTP = \frac{1}{|C|} \sum_{c \in C} TP_c \tag{7}$$

$$NDS = \frac{1}{10} \left[5mAP + \sum_{mTP \in TP} (1 - \min(1, mTP)) \right]$$

B. Implementation details

This paper implemented RCBEV on MMDetection3D [38], a well-conducted platform for 3D perception task. The model is trained on 4 NVIDIA GeForce GTX 3090 GPUs with 24GB memory. During the training process, AdamW optimizer [39]

is adopted to obtain optimized parameters. The learning rate is initialized to $2e - 4$. The training epoch is set as 20. And the total batch size is 32. Besides, we exploit CBGS [40], a class-balanced data grouping and sampling strategy during training for a more ideal result. The vision-branch backbone network of RCBEV is first pre-trained on the nuScenes dataset.

During training and testing, 6 cameras and 5 radars mounted on the vehicles are utilized for a more broad field of view. The image resolution is reduced from the original 1600×900 pixels to 704×256 pixels for a balance between precision and computational efficiency. We accumulate 10 sweeps of radar points to increase point cloud density. To further realize the data augmentation, random right-left or forward-backward flipping (with a probability of 0.5), random rotation (from -

TABLE II
PER-CLASS PERFORMANCE COMPARISONS FOR 3D OBJECT DETECTION ON nuSCENES DATASET.

Method	Modality	data	mAP↑									
			Car	Truck	Bus	Trailer	Const.	Pedest.	Motor.	Bicycle	Traff.	Barrier
BEVDet	Camera	val	0.508	0.222	0.311	0.150	0.073	0.336	0.262	0.213	0.506	0.502
BEVDet4d	Camera	val	0.536	0.247	0.335	0.160	0.079	0.384	0.292	0.278	0.546	0.522
RCBEV(Ours)	Camera+Radar	val	0.675	0.333	0.410	0.152	0.112	0.419	0.325	0.248	0.547	0.545
RCBEV4d(Ours)	Camera+Radar	val	0.683	0.323	0.369	0.148	0.108	0.443	0.357	0.270	0.552	0.557
mm-fusion	Camera+Radar	test	0.603	0.301	0.260	0.225	0.112	0.436	0.399	0.298	0.556	0.518
CenterFusion	Camera+Radar	test	0.509	0.258	0.234	0.235	0.077	0.370	0.314	0.201	0.575	0.484
RCBEV(Ours)	Camera+Radar	test	0.663	0.332	0.316	0.332	0.166	0.412	0.416	0.265	0.611	0.551

Ten categories include 'Car', 'Truck', 'Bus', 'Trailer', 'Construction vehicle', 'Pedestrian', 'Motorcycle', 'Bicycle', 'Traffic cone', 'Barrier'.

0.3925rad to 0.3925rad under LiDAR coordinate system), and random scaling (from 0.95 to 1.05 percent of point range) are implemented on radar point clouds. The voxel size is set to [0.1, 0.1, 0.2] meters towards the [x, y, z] directions.

C. Overall result analysis

The visible results of our method is shown in Fig 5. Five representative scenarios are selected from nuScenes dataset. At the top and medium part of the sub-picture, the ground truth (GT) of 3D bounding boxes are labeled in the front-view image and the bird-eye view. Then at the bottom part, our detection results are shown under BEV. The different colors of bounding boxes denote different object categories.

As for the quantitative analysis, we compare our radar and camera fusion 3D detection work RCBEV with the state-of-the-art camera-based method such as BEVDet [12] and BEVDet4d [41], and camera-radar fusion models like CenterFusion [8] on the nuScenes benchmark. As nuScenes dataset is split as training, validation and testing dataset, we use the training part for model training and evaluate the model performance on the validation and testing part.

Out of fairness and rigor, when evaluating our model on the validation set, the relevant factors which influence the performance were kept constant as much as possible. Consequently, the image size, and backbone of the vision-branch are kept the same among BEVDet, BEVDet4d, RCBEV and RCBEV4d. Here the image backbone and image neck are adopted as Swin-Transformer and FPN. When evaluating our model on the testing set, we upload our detection results and obtain the evaluation results from nuScenes evaluation server. We provide the highest results on the leaderboard under camera-radar modality, including the results of mm-fusion, CenterFusion and our works.

From Table I, we can see direct comparisons of different algorithms. Compared with the other methods, our method attains better performance in nearly all criteria. RCBEV outperforms BEVDet with 6.9% mAP and 7.9% NDS. And even when comparing with BEVDet4d, which imports temporal features of multiple images, RCBEV4d still overcomes with 3.9% mAP and 0.6% NDS. Then when we focus on the regression precision of location, rotation and dimension of objects, we find after utilizing radar information, the location

error, dimension error and velocity error of detection results, which are denoted by mATE, mASE, and mAVE achieve a significant reduction compared with BEVDet.

Besides, We receive the best performance on 3d detection task of camera-radar modality. On the validation set, RCBEV exceeds Centerfusion, the most representative public work on camera-radar fusion 3D detection with 4.5% mAP and 2.9% NDS. RCBEV4d exceeds Centerfusion with 4.9% mAP and 4.4% NDS. On the testing set, RCBEV receives the highest mAP score and NDS score with 40.6% and 48.6%. This demonstrates the superior performance of our fusion method compared with other camera-radar fusion works.

D. Evaluation on special cases

Table II displays the per-class performance of several methods mentioned above. As it is shown, compared with camera-only method, the accuracy of RCBEV has made great improvement on the following categories: car, truck, bus, construction vehicle, pedestrian, motorcycle, traffic cone and barrier. It is analyzed that radar data give more geometry constraints of objects which are useful to detection task.

Table III presents the performance of our fusion model and baseline model under different weather and lighting conditions. The metrics mAP and NDS get improved under sunny weather, rainy weather, daytime and night separately. Detection in the night and rainy weather is challenging for camera-only models due to the properties of camera lens. While radar owns stable working performance in adverse weather conditions, it improves the robustness of our detection model prominently.

E. Ablation study

In this section, ablation experiments are performed in the validation dataset to further prove the effectiveness of our proposed RCBEV. We control the variants of RCBEV design as is shown in Table IV-Table VI. The performance curve is visualized in Fig 6.

By comparing different image backbone networks in Table IV, the performance of Swin-Transformer and ResNet both get apparent improvement after fusing radar data. The NDS and mAP correspondingly increase (7.9%, 6.9%) and (12.3%,

TABLE III
THE ROBUST VALIDATION OF RCBEV IN DIFFERENT LIGHTING AND WEATHER CONDITIONS.

Method	Modality	Sunny		Rainy		Day		Night	
		mAP	NDS	mAP	NDS	mAP	NDS	mAP	NDS
BEVDet	C	0.304	0.391	0.318	0.462	0.312	0.407	0.134	0.231
RCBEV(Ours)	C+R	0.361	0.466	0.385	0.500	0.371	0.479	0.155	0.237
Difference Value		+5.7%	+7.5%	+6.7%	+3.8%	+5.9%	+7.2%	+2.1%	+0.6%

Notice that "C" and "R" specify camera and radar modalities respectively.

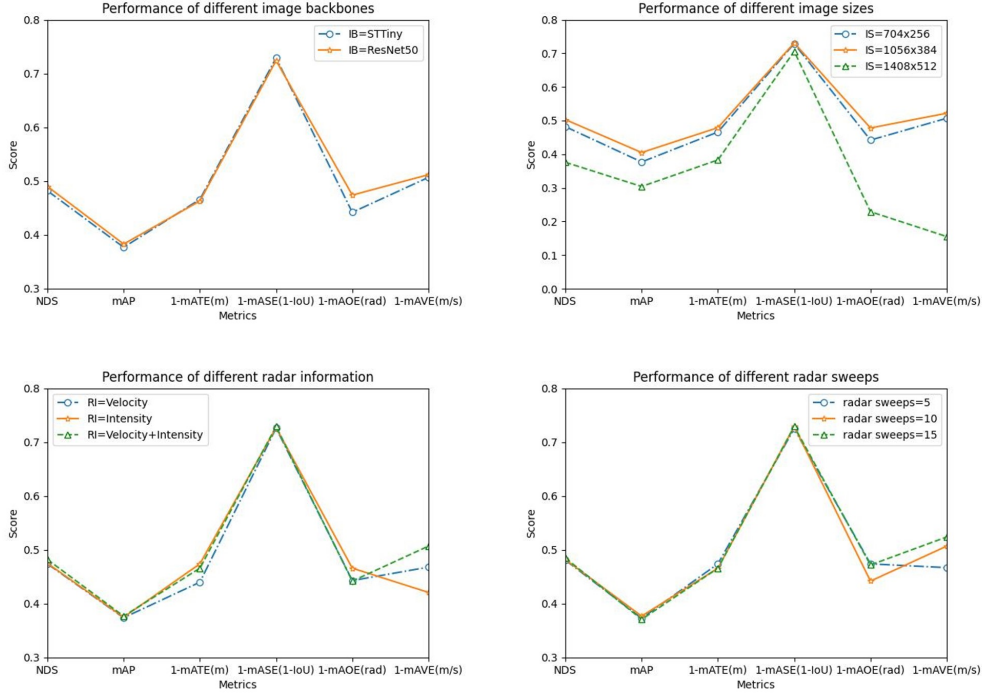


Fig. 6. The curves of model performance in the ablation study

8.4%). Hence it is confirmed that the fusion result can be better than the camera-only result with the same image backbone. As there exists a small distinction between performances of different backbone networks, this may be relevant to the different learning policies we adopt and different convergences of models.

By comparing different image resolutions in Table V, we can see that the best performance is carried out with 1056×384 image resolution. The highest performance is 50.3% NDS and 40.5% mAP. It is inferred that increasing image size suitably can increase the final performance. However, when exceeding the ideal range, the increase of image size will bring difficulty to the training process, which will do harm to the detection precision inversely.

Not only camera-related components but also radar-related components are discussed here. We change the properties which are used with position information to extract features in the radar-branch spatial encoder, and the detection performance is showed in Table VI. While both velocity and

intensity information is effective, the best performance is obtained by integrating them. Besides, it is indicated that the utilization of velocity information can reduce the error of velocity estimation in contrast with not using it.

Moreover, we change the number of sweeps we accumulated to extract features in the radar-branch temporal encoder, the result is showed in Table VII. According to the sampling frequency, 5,10,15 sweeps correspond to 1s, 2s, 2.5s approximately. It is figured out that more sweeps are good for the overall performance, especially velocity estimation.

From the comparisons of the above components, we can see that both radar-related and camera-related components have important influences on the final fusion performance. When choosing an appropriate feature extractor with suitable parameters, the fusion result will surpass the single-sensor model for certain.

TABLE IV
ABLATION EXPERIMENTS OF DIFFERENT IMAGE BACKBONES OF RCBEV ON nuSCENES

Backbone	Modality	NDS \uparrow	mAP \uparrow	mATE \downarrow	mASE \downarrow	mAOE \downarrow	mAVE \downarrow
STTiny	C	0.403	0.308	0.665	0.273	0.533	0.829
Resnet50	C	0.377	0.299	0.734	0.273	0.573	0.907
STTiny	R+C	0.482	0.377	0.534	0.271	0.558	0.493
Resnet50	R+C	0.490	0.383	0.537	0.276	0.526	0.488

TABLE V
ABLATION EXPERIMENTS OF DIFFERENT IMAGE SIZES OF RCBEV ON nuSCENES

Image size	NDS \uparrow	mAP \uparrow	mATE \downarrow	mASE \downarrow	mAOE \downarrow	mAVE \downarrow
704 \times 256	0.482	0.377	0.534	0.271	0.558	0.493
1056 \times 384	0.503	0.405	0.521	0.269	0.522	0.478
1408 \times 512	0.376	0.304	0.617	0.294	0.771	0.845

TABLE VI
ABLATION EXPERIMENTS OF RADAR INFORMATION OF RCBEV ON nuSCENES

radar data	NDS \uparrow	mAP \uparrow	mATE \downarrow	mASE \downarrow	mAOE \downarrow	mAVE \downarrow
V	0.474	0.374	0.560	0.274	0.557	0.532
I	0.475	0.375	0.526	0.273	0.534	0.579
V+I	0.482	0.377	0.534	0.271	0.558	0.493

TABLE VII
ABLATION EXPERIMENTS OF RADAR SWEEPS OF RCBEV ON nuSCENES

radar sweeps	NDS \uparrow	mAP \uparrow	mATE \downarrow	mASE \downarrow	mAOE \downarrow	mAVE \downarrow
5	0.481	0.373	0.526	0.275	0.526	0.533
10	0.482	0.377	0.534	0.271	0.558	0.493
15	0.485	0.371	0.534	0.271	0.528	0.476

VI. CONCLUSION

This paper proposed a novel radar-camera feature fusion 3D object detection method, which is called RCBEV. In contrast to the other fusion detection method with radar and camera, RCBEV bridge the view disparity of radar and camera features and realizes an efficient feature fusion system under the top-down view instead of the front view. Besides, aiming to the tough nut which comes from the sparsity and clutter of radar data, a radar temporal-spatial encoder is proposed to maximize the efficient information from radar points. Then our two-stage fusion method gives us a more sufficient information interaction during the fusion course to enhance the regression result. The model performance is validated on the large-scale benchmark nuScenes. Extensive experiments demonstrate that our method can successfully optimize the detection result compared with the baseline of image-only methods. What's more, the best detection performance has been achieved by RCBEV model among all the camera-radar fusion methods up to now.

RCBEV verified that by bridging the view disparity between image and radar data under the top-down view, obvious im-

provement on accuracy and robustness is able to be achieved. However, the current work still stays on the dynamic object perception task. Static elements in driving environment such as lane line, and lamp pole, which can be regarded as location marks and contribute to location and mapping in autonomous driving, have not been considered yet. As for future work, we will study how to utilize our fusion model to realize a unified perception of dynamic and static elements in driving scenes for the reconstruction of an integrated 3D environment. Besides, transfer learning of RCBEV needs to be considered with more field tests.

ACKNOWLEDGMENTS

This work was supported by the National Natural Science Foundation of China (U1864203, 52102396), and in part funded by the China Postdoctoral Science Foundation (2021M701897).

REFERENCES

- [1] X. Cai, M. Giallorenzo, and K. Sarabandi, "Machine learning-based target classification for mmw radar in autonomous driving," *IEEE Transactions on Intelligent Vehicles*, vol. 6, no. 4, pp. 678–689, 2021.
- [2] R. O. Chavez-Garcia and O. Aycard, "Multiple sensor fusion and classification for moving object detection and tracking," *IEEE Transactions on Intelligent Transportation Systems*, vol. 17, no. 2, pp. 525–534, 2015.
- [3] R. O. Chavez-Garcia, T.-D. Vu, and O. Aycard, "Fusion at detection level for frontal object perception," in *2014 IEEE Intelligent Vehicles Symposium Proceedings*. IEEE, 2014, pp. 1225–1230.
- [4] R. Nabati and H. Qi, "Rrpn: Radar region proposal network for object detection in autonomous vehicles," in *2019 IEEE International Conference on Image Processing (ICIP)*. IEEE, 2019, pp. 3093–3097.
- [5] G. Alessandretti, A. Broggi, and P. Cerri, "Vehicle and guard rail detection using radar and vision data fusion," *IEEE transactions on intelligent transportation systems*, vol. 8, no. 1, pp. 95–105, 2007.
- [6] R. Nabati and H. Qi, "Radar-camera sensor fusion for joint object detection and distance estimation in autonomous vehicles," *arXiv preprint arXiv:2009.08428*, 2020.
- [7] S. Chang, Y. Zhang, F. Zhang, X. Zhao, S. Huang, Z. Feng, and Z. Wei, "Spatial attention fusion for obstacle detection using mmwave radar and vision sensor," *Sensors*, vol. 20, no. 4, p. 956, 2020.
- [8] R. Nabati and H. Qi, "Centerfusion: Center-based radar and camera fusion for 3d object detection," in *Proceedings of the IEEE/CVF Winter Conference on Applications of Computer Vision*, 2021, pp. 1527–1536.
- [9] S. Chadwick, W. Maddern, and P. Newman, "Distant vehicle detection using radar and vision," in *2019 International Conference on Robotics and Automation (ICRA)*. IEEE, 2019, pp. 8311–8317.
- [10] T.-Y. Lim, A. Ansari, B. Major, D. Fontijne, M. Hamilton, R. Gowaikar, and S. Subramanian, "Radar and camera early fusion for vehicle detection in advanced driver assistance systems," in *Machine Learning for Autonomous Driving Workshop at the 33rd Conference on Neural Information Processing Systems*, vol. 2, 2019.
- [11] J. Philion and S. Fidler, "Lift, splat, shoot: Encoding images from arbitrary camera rigs by implicitly unprojecting to 3d," in *European Conference on Computer Vision*. Springer, 2020, pp. 194–210.
- [12] J. Huang, G. Huang, Z. Zhu, and D. Du, "Bevdet: High-performance multi-camera 3d object detection in bird-eye-view," *arXiv preprint arXiv:2112.11790*, 2021.
- [13] S. Shi, X. Wang, and H. Li, "Pointcnn: 3d object proposal generation and detection from point cloud," in *Proceedings of the IEEE/CVF conference on computer vision and pattern recognition*, 2019, pp. 770–779.
- [14] S. Shi, C. Guo, L. Jiang, Z. Wang, J. Shi, X. Wang, and H. Li, "Pv-rcnn: Point-voxel feature set abstraction for 3d object detection," in *Proceedings of the IEEE/CVF Conference on Computer Vision and Pattern Recognition*, 2020, pp. 10 529–10 538.
- [15] Y. Zhou and O. Tuzel, "Voxelnet: End-to-end learning for point cloud based 3d object detection," in *Proceedings of the IEEE conference on computer vision and pattern recognition*, 2018, pp. 4490–4499.

- [16] A. H. Lang, S. Vora, H. Caesar, L. Zhou, J. Yang, and O. Beijbom, "Pointpillars: Fast encoders for object detection from point clouds," in *Proceedings of the IEEE/CVF Conference on Computer Vision and Pattern Recognition*, 2019, pp. 12 697–12 705.
- [17] T. Yin, X. Zhou, and P. Krahenbuhl, "Center-based 3d object detection and tracking," in *Proceedings of the IEEE/CVF conference on computer vision and pattern recognition*, 2021, pp. 11 784–11 793.
- [18] Y. Wang and J. M. Solomon, "Object dgcnn: 3d object detection using dynamic graphs," *Advances in Neural Information Processing Systems*, vol. 34, 2021.
- [19] A. Mousavian, D. Anguelov, J. Flynn, and J. Kosecka, "3d bounding box estimation using deep learning and geometry," in *Proceedings of the IEEE conference on Computer Vision and Pattern Recognition*, 2017, pp. 7074–7082.
- [20] X. Weng and K. Kitani, "Monocular 3d object detection with pseudo-lidar point cloud," in *Proceedings of the IEEE/CVF International Conference on Computer Vision Workshops*, 2019, pp. 0–0.
- [21] T. Wang, X. Zhu, J. Pang, and D. Lin, "Fcos3d: Fully convolutional one-stage monocular 3d object detection," in *Proceedings of the IEEE/CVF International Conference on Computer Vision*, 2021, pp. 913–922.
- [22] X. Zhou, D. Wang, and P. Krähnenbühl, "Objects as points," *arXiv preprint arXiv:1904.07850*, 2019.
- [23] Y. Wang, V. C. Guizilini, T. Zhang, Y. Wang, H. Zhao, and J. Solomon, "Detr3d: 3d object detection from multi-view images via 3d-to-2d queries," in *Conference on Robot Learning*. PMLR, 2022, pp. 180–191.
- [24] Y. Liu, T. Wang, X. Zhang, and J. Sun, "Petr: Position embedding transformation for multi-view 3d object detection," *arXiv preprint arXiv:2203.05625*, 2022.
- [25] D. Rukhovich, A. Vorontsova, and A. Konushin, "Imvoxelnet: Image to voxels projection for monocular and multi-view general-purpose 3d object detection," in *Proceedings of the IEEE/CVF Winter Conference on Applications of Computer Vision*, 2022, pp. 2397–2406.
- [26] E. Xie, Z. Yu, D. Zhou, J. Phillion, A. Anandkumar, S. Fidler, P. Luo, and J. M. Alvarez, "M² 2bev: Multi-camera joint 3d detection and segmentation with unified birds-eye view representation," *arXiv preprint arXiv:2204.05088*, 2022.
- [27] S. Ren, K. He, R. Girshick, and J. Sun, "Faster r-cnn: Towards real-time object detection with region proposal networks," *Advances in neural information processing systems*, vol. 28, 2015.
- [28] J. Redmon, S. Divvala, R. Girshick, and A. Farhadi, "You only look once: Unified, real-time object detection," in *Proceedings of the IEEE conference on computer vision and pattern recognition*, 2016, pp. 779–788.
- [29] F. Nobis, M. Geisslinger, M. Weber, J. Betz, and M. Lienkamp, "A deep learning-based radar and camera sensor fusion architecture for object detection," in *2019 Sensor Data Fusion: Trends, Solutions, Applications (SDF)*. IEEE, 2019, pp. 1–7.
- [30] V. John and S. Mita, "Rvnet: deep sensor fusion of monocular camera and radar for image-based obstacle detection in challenging environments," in *Pacific-Rim Symposium on Image and Video Technology*. Springer, 2019, pp. 351–364.
- [31] O. Schumann, J. Lombacher, M. Hahn, C. Wöhler, and J. Dickmann, "Scene understanding with automotive radar," *IEEE Transactions on Intelligent Vehicles*, vol. 5, no. 2, pp. 188–203, 2019.
- [32] K. Cai, B. Wang, and C. X. Lu, "Autoplace: Robust place recognition with low-cost single-chip automotive radar," *arXiv preprint arXiv:2109.08652*, 2021.
- [33] Z. Liu, Y. Lin, Y. Cao, H. Hu, Y. Wei, Z. Zhang, S. Lin, and B. Guo, "Swin transformer: Hierarchical vision transformer using shifted windows," in *Proceedings of the IEEE/CVF International Conference on Computer Vision*, 2021, pp. 10012–10022.
- [34] T.-Y. Lin, P. Dollár, R. Girshick, K. He, B. Hariharan, and S. Belongie, "Feature pyramid networks for object detection," in *Proceedings of the IEEE conference on computer vision and pattern recognition*, 2017, pp. 2117–2125.
- [35] X. Shi, Z. Chen, H. Wang, D.-Y. Yeung, W.-K. Wong, and W.-c. Woo, "Convolutional lstm network: A machine learning approach for precipitation nowcasting," *Advances in neural information processing systems*, vol. 28, 2015.
- [36] K. He, X. Zhang, S. Ren, and J. Sun, "Deep residual learning for image recognition," in *Proceedings of the IEEE conference on computer vision and pattern recognition*, 2016, pp. 770–778.
- [37] H. Caesar, V. Bankiti, A. H. Lang, S. Vora, V. E. Liong, Q. Xu, A. Krishnan, Y. Pan, G. Baldan, and O. Beijbom, "nuscenes: A multimodal dataset for autonomous driving," in *Proceedings of the IEEE/CVF conference on computer vision and pattern recognition*, 2020, pp. 11 621–11 631.
- [38] M. Contributors, "Mmdetection3d: Openmlab next-generation platform for general 3d object detection," 2020.
- [39] I. Loshchilov and F. Hutter, "Decoupled weight decay regularization," *arXiv preprint arXiv:1711.05101*, 2017.
- [40] B. Zhu, Z. Jiang, X. Zhou, Z. Li, and G. Yu, "Class-balanced grouping and sampling for point cloud 3d object detection," *arXiv preprint arXiv:1908.09492*, 2019.
- [41] J. Huang and G. Huang, "Bevdet4d: Exploit temporal cues in multi-camera 3d object detection," *arXiv preprint arXiv:2203.17054*, 2022.

BIOGRAPHY SECTION

Taohua Zhou received the B.S. degree from Department of Automation, Tsinghua University, Beijing, China in 2018. She is currently working toward the Doctor degree at the School of Vehicle and Mobility, Tsinghua University, Beijing, China. Her research interests include object detection and tracking, information fusion, environmental perception of autonomous driving and vehicle-infrastructure cooperative perception.



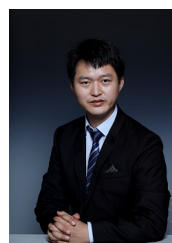
Yining Shi received the B.S. degree in School of Automotive Engineering from Tsinghua University, Beijing, China in 2021. He is currently working toward the Ph.D. degree at the School of Vehicle and Mobility in Tsinghua University, Beijing, China. His research interests include multi-modality 3D object detection and tracking, as well as grid-centric segmentation and motion prediction for autonomous driving.



Junjie Chen received the Ph.D. degree in traffic information engineering and control from the Beijing Jiaotong University in 2020. He was a Research Assistant at Carnegie Mellon University (CMU), Pittsburgh, PA, USA, from 2018 to 2020. He currently holds a post-doctoral position at the School of Vehicle and Mobility of Tsinghua University, Beijing, China. His research interests include nonparametric Bayesian learning, platoon operation control, and recognition and application of human driving characteristics.



Kun Jiang received the B.S. degree in mechanical and automation engineering from Shanghai Jiao Tong University, Shanghai, China in 2011. Then he received the Master degree in mechatronics system and the Ph.D. degree in information and systems technologies from University of Technology of Compiègne (UTC), Compiègne, France, in 2013 and 2016, respectively. He is currently an assistant research professor at Tsinghua University, Beijing, China. His research interests include autonomous vehicles, high precision digital map, and sensor



fusion.



Mengmeng Yang received the Ph.D. degree in Photogrammetry and Remote Sensing from Wuhan University, Wuhan, China in 2018. She is currently an assistant research professor at Tsinghua University, Beijing, China. Her research interests include autonomous vehicles, high precision digital map, and sensor fusion.



Diange Yang received his Ph.D. in Automotive Engineering from Tsinghua University in 2001. He is now a Professor at the school of vehicle and mobility at Tsinghua University. He currently serves as the director of the Tsinghua University Development & Planning Division. His research interests include autonomous driving, environment perception, and HD map. He has more than 180 technical publications and 100 patents. He received the National Technology Invention Award and Science and Technology Progress Award in 2010, 2013, 2018, and the Special

Prize for Progress in Science and Technology of China Automobile Industry in 2019.